Title

Mechanical injury and blood are drivers of spatial memory deficits after rapid intraventricular hemorrhage.

Authors

Kamal, Kimia
Keiter, Janet A
Binyamin, Tamar R
et al.

Publication Date

2020-11-01

DOI

10.1016/j.nbd.2020.105084

Peer reviewed

HHS Public Access

Author manuscript

Neurobiol Dis. Author manuscript; available in PMC 2021 November 01.

Published in final edited form as:

Neurobiol Dis. 2020 November ; 145: 105084. doi:10.1016/j.nbd.2020.105084.

Mechanical injury and blood are drivers of spatial memory deficits after rapid intraventricular hemorrhage

Kimia Kamal[1], **Janet A. Keiter**[2], **Tamar R. Binyamin**[1], **Joyce N. de la Cruz Dapula**[1], **Audrey R. Vergara**[1], **Cameron W. Hawk**[1], **Ali Izadi**[1], **Bruce Lyeth**[1], **Gene G. Gurkoff**[1], **Frank R. Sharp**[3], **Ben Waldau**[1]

[1]Department of Neurological Surgery, UC Davis Medical Center, Sacramento, CA 95817, USA

[2]Psychiatry and Behavioral Sciences, UC Davis Medical Center, Sacramento, CA, 95817, USA

[3]Department of Neurology, UC Davis Medical Center, Sacramento, CA, 95817, USA

Abstract

Aneurysmal intraventricular hemorrhage (IVH) survivors may recover with significant deficits in learning and memory. The goal of this study was to investigate the mechanism of memory decline after intraventricular aneurysm rupture. We developed an aneurysmal IVH rat model by injecting autologous, arterial blood over the period of two minutes into the right lateral ventricle. We also evaluated the effects of a volume-matched artificial cerebrospinal fluid (CSF) control, thrombin and the mode of delivery (pulsed hand injection versus continuous pump infusion). We performed magnetic resonance brain imaging after 1 and 5 weeks to evaluate for hydrocephalus and histological analysis of the dentate gyrus after 6 weeks. Only animals which underwent a whole blood pulsed hand injection had a spatial memory acquisition and retention deficit 5 weeks later. These animals had larger ventricles at 1 and 5 weeks than animals which underwent a continuous pump infusion of whole blood. We did not find a decline in dentate gyrus granule cell neurons or an impairment in dentate gyrus neurogenesis or differentiation 6 weeks after IVH. Rapid injections of blood or volume resulted in microglial activation in the dentate gyrus. In conclusion, our results point to mechanical injury as the predominant mechanism of memory decline after intraventricular aneurysmal rupture. However, volume-matched pulsed injections of artificial CSF did not create a spatial memory deficit at 5 weeks. Therefore, whole blood itself must play a role in the mechanism. Further research is required to evaluate whether the viscosity

Corresponding author: Ben Waldau, MD, Department of Neurological Surgery, UC Davis, 4680 Y Street, ACC 3740, Sacramento, CA 95817, USA, bwaldau@ucdavis.edu.

Credit author statement

KK: conceptualization, methodology, formal analysis, investigation, writing initial draft, visualization; JK: conceptualization, methodology, formal analysis, investigation, writing initial draft, visualization; TB: investigation; JD: formal analysis, writing initial draft; AV: formal analysis, writing initial draft; CH: formal analysis; AI: investigation; BL: investigation, writing review and editing; GG: formal analysis, visualization, writing review and editing; FS: methodology, writing review and editing, funding acquisition; BW: conceptualization, methodology, formal analysis, investigation, visualization, writing initial draft, writing review and editing, funding acquisition.

Conflict of interests

The authors declare no conflicts of interest.

of blood causes additional mechanical disruption and hydrocephalus through a primary injury mechanism or whether the toxicity of blood causes a secondary injury mechanism that leads to the observed spatial memory deficit after 5 weeks.

Introduction

Intraventricular hemorrhage (IVH) is a serious clinical problem that results in high morbidity, mortality and heavy socioeconomic burden[1–3]. IVH is characterized as the accumulation of blood in the ventricles of the brain and commonly occurs in adults from a hypertensive hemorrhage, ruptured aneurysm or arteriovenous malformation, or traumatic brain injury[4,5]. Reportedly, intracranial hemorrhage (ICH) has a global incidence rate of 12–15 per 100,000 cases yearly, of which 42–52% of adults develop IVH as a result of a spontaneous, non-traumatic ICH[4].

IVH in humans results in impairments in a range of cognitive domains such as language, executive function (i.e. planning, decision-making, and attention), and memory[1–4]. IVH is significantly associated with these severe neurocognitive disorders due to hydrocephalus and hippocampal injury[5]. Although the association between IVH and memory deficits are well-established, the exact mechanism of memory loss remains uncertain. Proposed mechanisms involve the cellular inflammatory response of the brain (microglia activation)[4,6,7] and the direct neurotoxic effects of blood and blood products on periventricular structures of the brain[3,4,8–11]. Blood products such as iron and thrombin can cause ependymal cell death, hippocampal injury and hydrocephalus[8–11]. Another possible mechanism of memory decline is acute hydrocephalus which can result in poor cognitive outcomes[3–5].

In a rat model of rapid intraventricular hemorrhage, we investigated potential mechanisms that result in spatial memory impairment. We analyzed the effects of IVH on spatial memory and examined correlations with pathological conditions such as hydrocephalus, impaired dentate neurogenesis and differentiation, neuronal cell death, and microglial activation to gain insight into potential mechanisms of IVH memory impairment. A deeper understanding of mechanisms will help develop therapies to prevent memory loss and improve the clinical outcome of IVH patients.

Materials and Methods

Animal surgery

The Institutional Animal Care and Use Committee (IACUC) of the University of California, Davis approved all animal use protocols and experimental procedures (IACUC protocol #20063). The project followed the ILAR Guide for the Care and Use of Laboratory Animals, IACUC policy on Surgery Guidelines for Rodents, and the UC Davis Animal Welfare Assurance on file with the US Public Health Service. We used male Sprague-Dawley rats (6–15 weeks of age; ENVIGO, Livermore, CA) weighing 275–380g for the study. The rats were first anesthetized with 3–5% Isoflurane (Henry Schein Animal Health, Dublin, OH) in an induction chamber and intubated. Afterwards, rats were intubated and ventilated using 1–3% Isoflurane and O2/N2O (1:2) carrier gas in order to maintain anesthesia and positioned

in a stereotaxic frame (Kopf Instruments, Tujunga, CA). Body temperatures were maintained at 37°C using an electrically heated pad with a rectal thermometer feedback. A scalp incision was made along the midline, and a bur hole was drilled. A 22-gauge ventricular cannula was stereotactically positioned (coordinates: 1.46 medial-lateral, −0.90 anterior-posterior, −4.60 dorsal-ventral, with respect to the bregma), and a 28-gauge ventricular needle was inserted into the right lateral ventricle (Plastics One Inc., Roanoke, VA).

The right femoral artery was catheterized to draw the blood sample. A 1.5–2.5 cm skin incision was made in the inguinal region on the right side. The femoral artery was identified and isolated from the vein and nerve. The distal end of the artery was ligated using sutures, and an aneurysm clip was placed in the proximal end of the artery to restrict blood flow prior to incision. An incision was then made close to the distal ligation site, and a silastic tube was inserted to aspirate arterial blood into a syringe. After the collection of blood, the tubing was removed, and both proximal and distal ends of the artery were ligated. Autologous blood (200 μl) was injected into the right lateral cerebral ventricle manually or with a pump over a two-minute interval. After 10 minutes, the ventricular needle was removed, and the skin incisions were closed with sutures. Once ambulatory, the animals were returned to their home cages with free access to food and water. After animals recovered from the procedure, no impairment in hind limb function was noted.

Experimental Groups

The study was divided into 4 experimental groups for the first cohort: Blood group, volume control group, thrombin group, and sham injection group. The blood group received 200 μl of autologous, arterial blood into the right lateral ventricle by a pulsed hand injection over two minutes. The naturally discontinuous movement of the thumb on the plunger of the syringe led to pulsed injections of approximately 20–50 μl at a time with intermittent pauses during the two-minute total injection interval (n=10). The volume control group, which was the control for the blood group, received 200 μl of artificial cerebrospinal fluid (aCSF, Sigma-Aldrich, St. Louis, MO, n=9). The thrombin group received 40 Units of bovine thrombin (Sigma-Aldrich; n=11) dissolved in 5 μl of aCSF, and the sham injection group received 5 μl aCSF (n=8). We dissolved bovine thrombin in 5 μl and not 200 μl because we specifically wanted to test the effect of thrombin without the confounding of volume. We chose bovine thrombin over rat thrombin based on previous results showing that intraventricular injection of bovine thrombin has a pathological effect on rats.[12] The needle was left in place for 10 minutes after all injections to prevent siphoning of the delivered product out of the ventricle with early removal of the needle. If no blood was injected, the femoral artery was catheterized and 200 μl blood was aspirated into a syringe but not injected. Animals underwent 5 days of intraperitoneal injection of BrdU (100 mg/kg) twice daily between days 7–11 to label dentate gyrus progenitor cells (Figure 1). Morris Water Maze was performed starting at day 28. Animals were perfused on day 42 and underwent histological examination of the dentate gyrus. Pulsed hand injections were repeated for a second cohort of animals to perform magnetic resonance imaging (MRI) of the brain around day 7 (blood group n=10; volume control group n=10; sham injection group n=9) and around day 35 (blood group n=4) after injury. A third cohort of animals underwent a continuous pump (kdScientific, model 100, Holliston, MA) infusion over two minutes as

opposed to pulsed hand injections. This cohort consisted of a naïve animal group (n=10), 200 μl blood group (n=10), a 200 μl artificial CSF volume control group (n=10) and 5 μl 40 Units of bovine thrombin group (n=10). Animals of this cohort underwent MRI brain around day 7 and day 35 after infusion.

Morris Water Maze

All animals were assessed for their acquisition of spatial memory learning on days 28–33 post-op in the Morris water maze (MWM). The test apparatus consisted of a large, white circular pool (183 cm diameter, 60 cm high) with a transparent, cylindrical platform (12.8 cm diameter, 20 cm high) placed inside the pool on the second quadrant (northeast side). The tank was filled with water to a depth of 23 cm, and the platform was submerged to a depth of 3 cm. Water temperature was maintained at 26±2 °C for the duration of the experiment. On each side of the testing room, there were unique visual cues to provide spatial landmarks for guidance in navigating the tank in search of the submerged platform. Rats were brought inside the testing room in pairs and were kept in a warmed holding cage. The experimenter was blinded to the animal group. Each animal received 4 trials per day, for 5 consecutive days, and was given 4-minute breaks in between each trial. In each trial, the rats were placed in a randomly selected location in the pool (North, South, East, West) and were allotted 120s to find the platform. Latency to reach the platform was recorded for each trial. Once they reached the platform, the rats were allowed to remain on the platform for 30s. If the rats failed to find the platform within 120s, the experimenter would manually guide them to the platform and allow them to stay for 30s. The rats were subjected to a probe trial on the sixth day. The probe trial consisted of the same set up as above except the platform was removed from the pool. The crossing times over the platform's previous location, percentage time in each quadrant as well as time in the 10% area of the total water maze around the platform were recorded. The 10% area proximal to platform refers to a concentric circle around the platform that covers 10% of the area of the water maze, as opposed to 25% percent of the water maze in the traditional target quadrant analysis[13]. Each trial was recorded using an overhead video camera (Logitech Webcam Software, Newark, CA) and analyzed offline with tracking software (ANY-maze, version 4.99, Stoelting Co., Wood Dale, IL). Mean latency of four trials to find the platform was calculated for each day to assess learning.

Magnetic Resonance Imaging and ventricular measurements

To visualize the effects of intraventricular injections on the brain, a second cohort of rats were subjected to a brain MRI scanning on weeks 1 and 5 after pulsed hand injection surgery. A brain MRI scan was performed on all animals in the study which underwent pump infusion as the third cohort. Rats were anesthetized with 3–5% isoflurane in an induction chamber and positioned in an imaging instrument. To maintain anesthesia during the procedure, rats were ventilated with 1–2.5% isoflurane and O_2 gas through a fitted nose cone. Body temperature and respiratory rate were monitored with a physiologic monitoring unit (SA Instruments, Stony Brook, NY) and a rectal thermometer. Imaging procedures were performed in a Biospec 7T MRI scanner (Bruker Biospin Corporation, San Jose, CA) provided by the UC Davis Center for Molecular and Genomic Imaging. Each image was

produced using a T2 fast echo sequence (repetition time/echo time= 6100/60 ms) with a field of view of 35 mm × 25 mm and 44 coronal slices.

Bilateral ventricular sizes were measured using ImageJ Analysis program by a blind observer. For each coronal slice, bilateral ventricles were outlined to measure the area. To calculate the ventricular volume, the areas of all the coronal slices from each image were summed up and multiplied by the section thickness (0.5 mm). Hydrocephalus was defined as a ventricular volume that was larger than the 95% confidence interval of the mean for the sham injection group (> 11.3 mm^3).

Immunohistochemistry

Six weeks after the surgery, animals were anesthetized and perfused via the aorta with ice-cold 4% paraformaldehyde (PFA) in phosphate buffer. Brains were removed, protected in 30% sucrose, snap-frozen and sectioned to 40 μm slices using a microtome. Five random rats from each treatment were randomly divided into 4 histology groups: BrdU/NeuN/GFAP, DCX/NeuN, NeuN and Iba1.

An antigen retrieval method was performed for BrdU immunohistochemistry. Sections were mounted onto Fisher SuperFrost Plus slides (Fisher Scientific), dried for 30 minutes and circled with a Pap pen (Vector Laboratories, Burlingame, CA). After three washes in 0.1M PBS, the sections were incubated with 2N HCl (Sigma-Aldrich) for 30 minutes at 37 degrees Celsius. Sections were subsequently incubated for two minutes in 0.1M sodium tetraborate at pH 8.5 and then washed three times in 0.1M PBS. Sections were blocked one hour at room temperature with blocking solution (10% horse serum (Sigma-Aldrich), 0.3% Triton-X (Sigma-Aldrich) in PBS. Primary antibodies used were Rat anti-BrdU 1:100 (Abcam, ab6326, lot 579883), Mouse anti-NeuN 1:200 (Millipore, MAB377, lot 2592741) and Rabbit anti-GFAP 1:200 (Abcam, ab7260, lot: R276454–2) in dilute blocking solution (2% horse serum, 0.06% Triton-X in PBS) for 48 hours at 4°C. Sections were washed three times in 0.1M PBS, rinsed with distilled water and incubated with secondary antibodies Goat anti-rat 488 1:500 (A11006, lot: 1689880), Goat anti-mouse 594 (A21424, lot: 784587) and Donkey anti-Rabbit 647 1:500 (Abcam, ab150075, lot: GR3191436–2) for two hours at room temperature. Sections were washed three times with 0.1M PBS, rinsed with distilled water and coverslipped with Fluoromount G (Southern Biotech, Birmingham, AL) or VectaShield with DAPI (Vector Shield Inc., Burlingame, CA).

For Doublecortin/NeuN dual immunolabeling, sections were mounted on SuperFrost plus slides, dried for 30 minutes, circled with a Pap pen and washed with HyClone (Logan, UT). Sections were blocked for 5 minutes in 1% BSA (Sigma-Aldrich) followed by blocking solution for 1 hour at room temperature with 5% Normal Goat Serum (Sigma-Aldrich) and 0.03% Triton-X100 (Sigma-Aldrich). Sections were incubated overnight at 4°C in blocking solution with Guinea pig polyclonal anti-Doublecortin 1:500 (Millipore, MAB2253) and Mouse monoclonal anti-NeuN 1:500 (Millipore, MAB377). The next day sections were washed in 0.1M PBS five times and incubated for 1 hour at room temperature with Goat anti-guinea pig 488 1:1000 (Vector Laboratories Inc.) and Goat anti-mouse 555 1:500 (Vector Laboratories Inc.). Sections were washed five times in PBS and mounted with VectaShield with DAPI.

The avidin-biotin-peroxidase complex (Vectastain Elite ABC Kit, Vector Laboratories, Inc., Burlingame, CA) method was used to perform NeuN immunohistochemistry for stereology. Brain sections were incubated at room temperature in 0.3% H_2O_2 in methanol for 30 min to quench endogenous peroxidase. After two 5 min rinses in PBS, sections were incubated with 3% horse blocking serum for 20 min, and then incubated for 0.5 h in primary antibody (mouse anti-NeuN, 1:150, Millipore MAB377, Billerica, MA) diluted in PBS containing 0.1% Triton X-100 and 3% horse serum. After a wash in PBS, sections were incubated in biotinylated secondary antibody (Goat anti-mouse 1:1000, Vector BA 9200, Burlingame, CA) for 30 minutes. After three 5 min rinses in PBS, sections were placed in Vectastain ABC reagent for 30 minutes. After two more 5 min washes, sections were incubated in peroxidase substrate 3,3'-diaminobenzidine (DAB, Vector Shield Inc., Burlingame, CA) solution for 10 min. DAB staining was examined using a Nikon E600 microscope.

Immunofluorescence staining for microglia was performed with Rabbit anti-Iba1 primary antibody (1:1000; Wako, cat# 019–19741) followed by secondary antibody of Donkey anti-rabbit AF647 (1:500, Abcam, cat# 150075). Immunohistochemistry for Iba1 stereology utilized the same primary antibody followed by biotinylated goat anti-rabbit (1:200, Vector Shield Inc.) and DAB visualization method described above for NeuN immunolabeling.

Hematoxylin and Eosin staining was performed according to a slightly modified version of previously published protocols.[14] Primary antibodies for immunohistochemical evaluation of the ependymal surface were Rabbit anti-GFAP (1:200, Sigma, Cat# G9269) and Mouse anti-β-catenin (1:200, BD Biosciences, Cat# 610153).

Stereology of NeuN and Iba1 in the dentate gyrus and other quantification

The investigator was blinded to the group. Tissue was examined on a microscope (Nikon E600) with a motorized stage (MAC5000 System; Ludl Electronic Products, Ltd., Hawthorne, NY) using computer software (Stereo Investigator™ 2019 1.2; Microbrightfield, Inc., Williston, VT). In brief, Stereo Investigator is a software that uses random, unbiased frames over regions of interest. Prior to counting aggregates or cells, the number of sections, thickness (40 μm), and the interval between sections (five) were added to this software. For analysis of the dentate gyrus, we evaluated every fifth section (ssf = 0.2) between ~−2.56 bregma (first section where both blades of the dentate come together) to ~−4.52 bregma (prior to the fusion of the dorsal and ventral hippocampus). For the probe selection, dentate gyrus granule cell layer boundaries were traced for NeuN, and the dentate hilus boundaries were traced for Iba1 at 10x magnification (Plan Apo, NA 0.45; Nikon). The dentate hilus was defined as the area between the two blades of the dentate gyrus granule cell layer and a vertical line drawn between the two distal ends of the granule cell layer. Tissue was then examined at optimal magnification (microscope Nikon Eclipse E600, 100x, Oil lens). NeuN and Iba-1-positive cells were counted by placing a marker on each cell if it was at least 50% within the counting frame and not touching the red exclusion line. Stereology for NeuN in the granule cell layer of the dentate gyrus was performed with a grid size of 160 μm^2, counting frame of 15 μm^2 and section mounted thickness of 10 μm (asf = 0.0088 μm; hsf = 0.22 μm). Stereology for Iba1 in the dentate hilus was performed with a grid size of 200 μm^2, counting frame of 60 μm^2 and section mounted thickness of 10 μm (asf = 0.09 μm; hsf

= 0.22 μm). BrdU-, BrdU/NeuN-, BrdU/GFAP- and doublecortin-positive cells were counted in the entire subgranular zone of the dentate gyrus between the stereotactic coordinates described above. No stereology needed to be performed for BrdU, BrdU/NeuN, BrdU/GFAP and doublecortin since we were able to directly count the total number of cells in the region of interest.

Fractal Analysis using FracLac for ImageJ.

FracLac is a computer-aided morphological analysis which quantifies cell complexity (fractal dimension, D_b) and rotational heterogeneity (lacunarity, Λ), and is a widely accepted method to identify transitional morphologies ranging from amoeboid to complex branched. FracLac requires binary images of individual cells, therefore we took stacked immunofluorescent confocal images of Iba1-positive cells in the hilus of the dentate gyrus with a total z depth of 20 microns (11 images at 2 microns apart) at 25x; they were then stacked and merged for 2D visualization. The 2D image was then thresholded uniformly, carefully cropped, made into binary images and processed using the FracLac plugin for ImageJ. All microglia within the hilus of the dentate gyrus for both hemispheres were chosen for analysis as long as they were not overlapping with neighboring cells, and they appeared to have complete nucleus and branches yielding more than 100 cells from 3 animals from each treatment group (335, 331, and 380 cells total for sham control, volume control, and IVH respectively). All sections were uniformly stained and clear of background. FracLac uses a sliding box of decreasing size to determine the amount of pixel detail with each decreasing scale. In other words, a microglial cell is considered more complex if the amount of detail or pixels grows quickly as the scale increases, or as fractal dimension (D_b) approaches 2. We performed the fractal and lacunarity analysis using the average of 12 measurements with different and random placement of the grid. For a more detailed reference and explanation of FracLac and these measures please refer to the guide provided for FracLac at http://rsb.info.nih.gov/ij/plugins/fraclac/FLHelp/Introduction.htm and additional associated references (Karperien, A., FracLac for ImageJ1 1999–2013; available at the ImageJ website, National Institutes of Health).

Statistical Analysis

For water maze analysis, statistical differences were determined using repeated measures ANOVA with assessment days as the repeated variable within subjects followed by Dunnett's post hoc test. For the probe trial, time in each region (10% concentric circle and the 25% quadrant) as well as latency to enter the target quadrant were evaluated with a one-way ANOVA and post hoc Bonferroni multiple comparisons.

Hand-injection MRI volumetric data after 1 week was analyzed with Dunn's multiple comparison test. A Wilcoxon matched-pairs signed rank test was used to compare ventricular volumes for intraventricular blood injections after 1 and 5 weeks. Pump-infusion MRI volumetric data was analyzed with a Kruskal-Wallis H test after 1 and 5 weeks.

Ordinary one-way ANOVAs were performed to compare cells counts for BrdU, NeuN and Iba-1 because these cell counts passed the normality test of Kolmogorov-Smirnov. A Kruskal-Wallis H test was performed to test DCX cell counts for significant differences. For

BrdU and DCX, total counts per dentate gyrus were compared between groups. For NeuN, total counts per animal were compared between groups.

Data for fractal dimension and lacunarity was analysed in Python (Python Software foundation, Wilmington, Delaware) using custom scripts and freely available SciPy, pandas and matplotlib libraries. We performed a Kruskal-Wallis ANOVA followed by a Mann-Whitney U test with a Bonferroni correction, for multiple comparisons, due to the non-parametric nature of the data and therefore the results are shown as median (IQR) values. Normality was tested with Kolmogorov-Smirnov. A p value of < 0.05 was considered significant.

Results

Pulsed whole blood injections result in impaired memory acquisition and retention in Morris Water Maze.

First, we tested whether rapid intraventricular injections of 200 μl blood or artificial CSF, or 5 μl of thrombin or artificial CSF cause a deficit in learning and memory 5 weeks after the injection. There was a main effect of day ($F_{(4, 136)}= 61.45$, $p < 0.001$) to find the hidden platform indicating spatial learning in all groups so animals were able to learn the location of the platform (Figure 2A). There was no main effect of group on latency to find the platform in Morris Water Maze during acquisition ($F_{(3. 34)}= 2.22$, $p= 0.1$); Figure 2A). There was a significant interaction between day and group ($F_{(12, 136)} = 1.86$, $p < 0.05$). Only blood injection was different from sham in latency to find the platform (Dunnett's posthoc analysis, $p < 0.05$). No difference in swim speed were recorded among groups (Figure 2B). For the probe trial analysis, two rats in the IVH group were identified as outliers using the ROUT method with a false discovery rate of 2% and eliminated from analysis. Although the probe trial data showed that all groups, including blood, significantly spent more time in the platform quadrant in the traditional probe trial (Figure 2C), there was a significant main effect of group on time spent in the 10% of the total water maze area concentric circle around the platform ($F_{(3, 32)}= 4.37$, $p=<0.05$; Figure 2D). Rats with intraventricular blood spent significantly less time in the 10% circular area around the platform than rats that received a sham injection (Dunnett's posthoc, $p <0.05$).

Rats with pulsed injections of intraventricular blood develop persistently enlarged lateral ventricles—Next, we analyzed whether the different treatment groups developed hydrocephalus after pulsed hand injections as a possible explanation for the memory impairment in Morris water maze. Nine of 10 rats in the blood injection group were found to have hydrocephalus after 1 week on MRI brain. Rats which underwent pulsed hand injections of blood developed larger ventricular volumes after 1 week (median=24.61 mm^3, interquartile range (IQR)=15.67–36.97 mm^3, Figure 3A) than animals with a volume-matched artificial CSF injection (median 14.28 mm^3, IQR=12.09–23.81 mm^3, Figure 3B) and sham-injected animals (median 7.516 mm^3, IQR= 5.136–10.98 mm^3, Figure 3C). A Dunn's multiple comparisons test showed a significant difference in ventricular sizes between blood injections and sham injections ($p=0.0005$) and volume control injections and sham injections ($p=0.0382$; Figure 3D). In four animals, ventricular volumes after

intraventricular blood injections did not significantly change from week 1 to week 5, the time of the Morris water maze testing (median 19.11 mm^3, IQR = 12.34–43.24 mm^3 versus median 22.29 mm^3, IQR = 11.89–35.71 mm^3; p = 0.8750; Figure 3E). Therefore, rats after intraventricular hemorrhage still had persistent hydrocephalus 5 weeks after injection.

Steady-state pump infusion of blood into the lateral ventricle over two minutes does not cause a spatial memory deficit—In order to understand if pulsed injections cause the spatial memory deficit through spikes in intracranial pressure and mechanical disruption, we performed continuous pump infusions in the experimental groups over the same time interval as the hand injections were carried out. In contrast to the pulsed hand injections, we did not detect a spatial memory deficit in the acquisition phase (Figure 4A) or in the probe trial (data not shown) across all experimental groups, including autologous blood injections (n=10 for each group). Even though animals did not show spatial memory deficits, on 1-week follow-up MRI brain we found hydrocephalus in animals receiving blood infusion (Figure 4B) but not in animals after volume control (Figure 4C) or sham infusions (Figure 4D). Animals 1 week after blood infusion had significantly larger ventricles (median 20.18 mm^3, IQR = 12.6–25.68 mm^3) than animals after volume control infusion (median 11.73 mm^3, IQR = 10.62–13.57 mm^3) and thrombin infusion (median 12.79 mm^3, IQR = 11.24–16.51 mm^3; H = 7.173, 2 d.f., p = 0.0277; Figure 4E). Five weeks later, animals after blood infusions continued to have significantly larger ventricles (median 22.78 mm^3, IQR = 18.14–28.73 mm^3) than after volume control (median 11.24 mm^3, IQR = 9.65–15.68 mm^3) and thrombin infusions (17.82 mm^3, IQR = 12.86–21.22 mm^3; H = 7.951, 2 d.f., p = 0.0097; Figure 4F). Therefore, animals showed persistent hydrocephalus at the time of water maze testing after whole blood infusions, but the observed degree of hydrocephalus did not result in a spatial memory deficit.

Histological evaluation of dentate gyrus neuronal survival and neurogenesis after IVH—Next, we evaluated whether IVH contributes to neuronal cell death in the granular zone of the dentate gyrus or to impairment in dentate gyrus neurogenesis or progenitor cell differentiation by performing immunohistochemistry for NeuN, BrdU, BrdU/NeuN, BrdU/GFAP and DCX (Figure 5). We did not find a significantly decreased number of neurons in the granular zone of the dentate gyrus 5 weeks after injury with stereology (148946.48 ± 34001.87 estimated cells per region of interest after blood injection; 163441.77 ± 23573.16 estimated cells per region of interest after volume control injection; 160927.28 ± 23611.41 estimated cells per region of interest for sham injection; $F_{(2, 12)}$ = 0.3, p = 0.68; Figure 6A). Therefore, we did not have evidence for neuronal death in the dentate gyrus after intraventricular blood. Likewise, the number of BrdU-positive cells per 40 μm section in the region of interest was not significantly different across the treatment groups (108.21 ± 49.05 cells per 40 μm section in region of interest after blood injection; $F_{(2, 151)}$ = 0.45, p = 0.64; 105.43 ± 39.23 cells per 40 μm section in region of interest after volume control injection; 113.31 ± 37.79 cells per 40 μm section in region of interest after sham injection; Figure 6B). A high number of dentate progenitor cells continued to differentiate into neurons after intraventricular blood so differentiation capacity did not seem to be impaired (median 93.09%, IQR=91.18–95% differentiation into NeuN; median 5.44%, IQR=5–5.88% differentiation into GFAP; median 1.47%, IQR=0–2.94% no

differentiation; Figure 6C). There was also not a significant difference in the number of doublecortin-positive dentate progenitor cells between the groups (median 13 (IQR = 9–16) cells per 40 μm section in region of interest after blood injection; median 12 (IQR = 8–16) cells per 40 μm section in region of interest after volume control injection; 13 (IQR = 7.25–16.75) cells per 40 μm section in region of interest after sham injection; H = 1.842, 2 d.f., p = 0.3981; Figure 6D).

Pulsed injections of blood or artificial CSF cause microglial activation.

We next assessed the possibility that activated microglia may serve as a potential mechanism of IVH memory impairment. We first analyzed whether pulsed injections of blood or aCSF altered the number of microglia within the dentate gyrus. Using a stereological counting approach, we counted the number of Iba1 positive microglia within the dentate gyrus after 6 weeks (Figure 7ABC). None of the groups were statistically different from each other. The sham injected animals (13672 ± 6114; Figure 7D) did not show any more or less microglia statistically than either aCSF-injected (16233 ± 7259) or blood-injected animals (16704 ± 7470). Previous work has linked microglial activation to secondary brain injury as a possible mechanism contributing to cognitive deficits. Due to the close association between microglia, neurons and neuronal progenitors, it is likely that altered microglial function as represented by altered morphology will impact normal neuronal function. Therefore, we assessed changes in microglial morphology as a proxy for microglial activation using published methods[15]. We were able to measure the overall complexity of each microglia with two separate measures, lacunarity and fractal dimension, utilizing Iba1-positive immunofluorescent images, thresholded and binarized (Figure 7E). In the case of lacunarity we saw a statistically significant increase ($p < 0.05$) with pulsed injections for both volume control (median 1.0385, IQR=0.9197–1.1872) and blood (median 1.05945, IQR=0.9281–1.2216) over sham injection controls (median 0.9348 IQR=0.83225 – 1.0742; Figure 7F). The increase in lacunarity means that pulsed injections are causing morphological changes in the microglia where they have more gaps between processes and exhibit less symmetry around the cell body. Fractal analysis measures the overall complexity in morphology resulting in fractal dimension values that range from 1–2, where 1 is a straight line and 2 is a fractal with infinite complexity. In the case of fractal dimension values we saw a statistically significant decrease ($p < 0.05$) with pulsed injections for both volume control (median 1.4227, IQR=1.3725–1.4644) and blood (median 1.42365, IQR=1.377925–1.468325) over sham controls (median 1.4469, IQR=1.40885–1.48135; Figure 7G). The decrease in fractal dimension combined with the increase in lacunarity emphasizes that pulsed whole blood and volume control injections shift the microglia to a less complex morphology suggesting microglial activation persists up to 5 weeks post injury.

Pulsed hand injections do not cause microscopic ependymal injury—To address the question whether pulsed injections cause microscopic ependymal disruption or scarring, we qualitatively examined the surface of the lateral ventricle. Neither Hematoxylin & Eosin staining nor immunohistochemical labeling with GFAP/β-Catenin showed microscopic evidence for gross mechanical disruption or scarring of the ependyma 5 weeks after the injury when representative images for each group were sampled from the same regions of the medial ventricular wall (Figure 8).

Discussion

The present experimental study aims to understand the mechanistic framework of aneurysmal IVH and how it produces neurocognitive deficits. For this purpose, we developed an aneurysmal IVH rat model which we based off a previous model which involved slower infusion rates and venous blood[11]. We were able to show that rapid, pulsed intraventricular injections of autologous arterial blood produce spatial memory acquisition and retention deficits. We subsequently evaluated the possible underlying mechanism of the spatial memory decline. We started the experimental work with the hypothesis that IVH may lead to neurotoxicity in the dentate gyrus specifically affecting dentate gyrus neurogenesis. However, we found that dentate gyrus neurogenesis and neuronal survival were unaffected by IVH. Our results of dentate gyrus neurogenesis after IVH are in agreement with two previous studies examining dentate neurogenesis after SAH. Both studies found a decrease in dentate gyrus neurogenesis within one week after subarachnoid hemorrhage, but normal levels of neurogenesis returned after 7 days[16,17]. We did not find a change in dentate progenitor differentiation fate with blood since most progenitor cells after 1 week had differentiated into neurons 5 weeks later. Our finding is in agreement with Mino et al. who showed that the majority of BrdU-positive cells migrating into the granule cell layer had differentiated into NeuN-positive cells 30 days after subarachnoid hemorrhage[17]. Since we measured our spatial memory deficits 5 weeks after IVH, we conclude that the observed spatial memory impairment was not caused by impaired dentate gyrus neurogenesis. We can also refute the hypothesis that IVH decreases the resident pool of dentate progenitor cells through forced terminal differentiation since the number of doublecortin-positive cells at 42 days was unchanged. We only detected a spatial memory deficit after 5 weeks if injections were manually pulsed and not after continuous infusion of whole blood. This subtle difference in technique gave us important information on the possible mechanism of the memory decline. The mechanism of the memory decline may arise from a rapid surge in intracranial pressure (ICP) during the naturally discontinuous and therefore more disruptive hand injections. Another indication that mechanical disruption is a main driver of the memory deficit comes from initial experiments in which four out of five (80%) of animals died after a one-minute injection of blood into the lateral ventricle (data not shown). Therefore, it is likely that a hand injection causes mechanical disruption similar to traumatic brain injury, and the observed deficit may be similar to the deficit observed after traumatic brain injury. Even mild traumatic brain injury can lead to spatial learning deficits in cortical impact models[18]. In addition, permanent forniceal injury and reorganization has been documented in patients after TBI[19,20]. The fornix is adjacent to the lateral ventricle. It is possible that the impact of the whole blood injection lead to a forniceal stretch injury that was more pronounced with rapid ventricular expansion and ICP spikes with the hand injection as opposed to the slower ventricular expansion with the continuous pump infusion. In support of this hypothesis, we saw larger ventricular volumes after hand injections than pump infusions (median approximately 25 mm^3 with hand injection versus approximately 20 mm^3 with pump infusion), and we frequently observed bilateral ventricular dilatations with hand injections compared to unilateral ventricular dilatations with continuous pump infusion. It is therefore possible that rapid bilateral ventricular dilatation is required to create forniceal stretch injury and the resulting spatial memory deficit.

We found that resident microglia in the dentate gyrus exhibited activated morphologies after both whole blood and volume-matched pulsed hand injections supporting the hypothesis that trauma from mechanical disruption drives a persistent change in microglial activity. Numerous studies have found similar microglial activation after various types of brain insult, specifically after traumatic brain injury (TBI).[21,22] However, since volume-matched injections that exhibited microglial activation did not also exhibit spatial memory deficits, we cannot correlate the two. These findings may suggest that either microglial activation is not acting alone or that microglia are differentially activated in a way not reflected in their morphology. Microglia have been shown to play an active role in adult hippocampal neurogenesis. While in our experiments we did not see changes in neurogenesis, it is possible that primed or sensitive microglia may differentially influence the homeostatic relationship between neurons and microglia. Activated microglia, as assessed by decreasing complexity in morphology, have previously been shown to secrete neuron altering and neurotoxic factors. In addition, studies have shown that homeostatic or non-activated microglia play a regulatory role in neuronal connectivity through such mechanisms as direct synapse elimination and conversely synapse strengthening.[23–26] These studies have directly correlated these microglial activities to cognitive deficits. While assessing microglial morphological changes as a proxy for functional changes is not perfect, it can reveal categorical changes and serve as a good starting point for further analysis.[15]

Animals in our aneurysmal IVH model developed hydrocephalus, which replicates previous studies[10,27]. Hydrocephalus causes brain injury through various mechanisms such as inflammation, brain edema or impairment in regional cerebral blood flow[27–29]. Chen et al.[5,8] showed that intracerebral hemorrhage with ventricular extension resulted in more hydrocephalus than a volume-matched injection into the ventricle only, which may be explained by disruption of the ependyma. In our study however, we did not find ependymal disruption. Olopade et al. showed a relationship between severity of hydrocephalus and neurobehavioral changes including spatial memory deficits[30]. Their findings are consistent with our observations since we found that animals with milder hydrocephalus after pump infusions did not have a spatial memory deficit, whereas animals with more severe hydrocephalus after hand injection did develop a deficit. It is unclear however whether hydrocephalus itself causes the spatial memory deficit or whether the presence of hydrocephalus is a surrogate marker of other brain injury such as forniceal stretch injury. Pediatric patients with hydrocephalus can still develop high intelligence[31]. The clinical picture may be different in adults who do not have sufficient plasticity to compensate. In addition, the onset of hydrocephalus may be more rapid in adults after IVH than in children with other clinical causes. Adult rat hippocampal slice culture experiments have shown that 5% strain injury is sufficient to cause electrophysiological dysfunction, and the CA3 region, which connects with the fornix, is the most vulnerable to stretch injury[32]. Another group demonstrated that a strain of 21% caused electrophysiological changes, while a strain of 34% caused white matter injury[33]. Some pediatric patients with slowly developing hydrocephalus may not have axonal injury since a strain of 100% is tolerated without electrophysiological dysfunction when slower mechanical loading rates are applied[34].

An important question is how much the toxicity of the blood itself contributed to the spatial memory deficit. Neural toxicity of blood has been established in numerous studies, either

through hemoglobin[35,36], iron[9,37], ferritin[38], thrombin[10,11] or oxidative stress[39]. However, we did not see any water maze deficits with pump infusion with whole blood arguing against the hypothesis that blood toxicity is the driver of the spatial memory deficit. We used artificial CSF as volume control, but artificial CSF does not have the same viscosity as blood. It is possible that artificial CSF quickly redistributed along the needle track into the subarachnoid space during the rapid injection whereas whole blood was too viscous for such a rapid redistribution. Rapid redistribution of artificial CSF along the needle track may have dampened the pressure wave of the injection and put less stress on the forniceal columns whereas the viscosity of the blood lead to greater local mechanical disruption by causing higher ICP spikes. Another possibility is that the viscosity and coagulation of the blood in the syringe created more abrupt hand movements due to increased resistance compared to artificial CSF which could be injected more smoothly by hand into the lateral ventricle due to a lower resistance. Yet another explanation is that we did not see a spatial memory deficit with pump infusion of blood since the ependyma was not injured enough for the blood products to penetrate into the interstitial space and exert their neurotoxic effects. This mechanism would entail a primary injury to the ependyma by mechanical disruption followed by a secondary injury from blood product toxicity. On our examination of the ependymal surface however, we did not see evidence for microscopic disruption of tissue in any group after 5 weeks. It is possible though that the ependyma had healed by that time. Nevertheless, blood in the ventricle causes hydrocephalus since ventricles were significantly larger after continuous blood infusion than after volume control infusion through the pump so a primary/secondary insult mechanism through blood toxicity may be more likely. One of the weaknesses of our model is the large variability in ventricular volumes due to the natural variability of pulsed hand injections. However, even with the large range of ventricular sizes with pulsed hand injections, our MRI brain volumetric differences were very significant. Experimental variations may be decreased in future experiments by trialing the pump at higher velocities to simulate the force of a hand injection. A further limitation includes the exclusive use of male rats for the study to avoid the estrous cycle as an additional confounder for water maze results.

Conclusion

Pulsed injections of 200 μl whole blood over 2 minutes into the lateral ventricle create a spatial memory deficit at 5 weeks, while a continuous infusion of whole blood over the same time period does not. However, volume-matched pulsed injections of artificial CSF also do not create a spatial memory deficit at 5 weeks. Therefore, we identified the presence of blood and pulsed injections as the drivers of spatial memory deficit after intraventricular hemorrhage. Further research is required to evaluate whether the viscosity of blood causes additional mechanical disruption through a primary injury or whether the toxicity of blood causes a secondary injury that leads to the observed spatial memory deficit after 5 weeks.

Acknowledgements

This research was founded by NIH grant K08NS105914.

References

1. Al-Khindi T, Macdonald RL & Schweizer TA Cognitive and functional outcome after aneurysmal subarachnoid hemorrhage. Stroke 41, e519–536, doi:10.1161/STROKEAHA.110.581975 (2010). [PubMed: 20595669]
2. Kreiter KTet al.Predictors of cognitive dysfunction after subarachnoid hemorrhage. Stroke33, 200–208, doi:10.1161/hs0102.101080 (2002). [PubMed: 11779911]
3. Zanaty Met al.Intraventricular extension of an aneurysmal subarachnoid hemorrhage is an independent predictor of a worse functional outcome. Clin Neurol Neurosurg170, 67–72, doi:10.1016/j.clineuro.2018.04.032 (2018). [PubMed: 29730271]
4. Strahle Jet al.Mechanisms of hydrocephalus after neonatal and adult intraventricular hemorrhage. Transl Stroke Res3, 25–38, doi:10.1007/s12975-012-0182-9 (2012). [PubMed: 23976902]
5. Chen Qet al.Chronic hydrocephalus and perihematomal tissue injury developed in a rat model of intracerebral hemorrhage with ventricular extension. Transl Stroke Res6, 125–132, doi:10.1007/s12975-014-0367-5 (2015). [PubMed: 25167916]
6. Schneider UCet al.Microglia inflict delayed brain injury after subarachnoid hemorrhage. Acta Neuropathol130, 215–231, doi:10.1007/s00401-015-1440-1 (2015). [PubMed: 25956409]
7. Lull ME & Block ML Microglial activation and chronic neurodegeneration. Neurotherapeutics 7, 354–365, doi:10.1016/j.nurt.2010.05.014 (2010). [PubMed: 20880500]
8. Chen Qet al.Intracerebral Hematoma Contributes to Hydrocephalus After Intraventricular Hemorrhage via Aggravating Iron Accumulation. Stroke46, 2902–2908, doi:10.1161/STROKEAHA.115.009713 (2015). [PubMed: 26265129]
9. Gao Cet al.Role of red blood cell lysis and iron in hydrocephalus after intraventricular hemorrhage. J Cereb Blood Flow Metab34, 1070–1075, doi:10.1038/jcbfm.2014.56 (2014). [PubMed: 24667910]
10. Gao Fet al.Hydrocephalus after intraventricular hemorrhage: the role of thrombin. J Cereb Blood Flow Metab34, 489–494, doi:10.1038/jcbfm.2013.225 (2014). [PubMed: 24326390]
11. Liu DZet al.Inhibition of Src family kinases improves cognitive function after intraventricular hemorrhage or intraventricular thrombin. J Cereb Blood Flow Metab37, 2359–2367, doi:10.1177/0271678X16666291 (2017). [PubMed: 27624844]
12. Liu DZet al.Blood-brain barrier breakdown and repair by Src after thrombin-induced injury. Ann Neurol67, 526–533, doi:10.1002/ana.21924 (2010). [PubMed: 20437588]
13. Kolarik BSet al.Impairments in precision, rather than spatial strategy, characterize performance on the virtual Morris Water Maze: A case study. Neuropsychologia80, 90–101, doi:10.1016/j.neuropsychologia.2015.11.013 (2016). [PubMed: 26593960]
14. Cardiff RD, Miller CH & Munn RJ Manual hematoxylin and eosin staining of mouse tissue sections. Cold Spring Harb Protoc 2014, 655–658, doi:10.1101/pdb.prot073411 (2014). [PubMed: 24890205]
15. Karperien A, Ahammer H & Jelinek HF Quantitating the subtleties of microglial morphology with fractal analysis. Front Cell Neurosci 7, 3, doi:10.3389/fncel.2013.00003 (2013). [PubMed: 23386810]
16. Zuo Yet al.Neurogenesis changes and the fate of progenitor cells after subarachnoid hemorrhage in rats. Exp Neurol311, 274–284, doi:10.1016/j.expneurol.2018.10.011 (2019). [PubMed: 30359565]
17. Mino Met al.Temporal changes of neurogenesis in the mouse hippocampus after experimental subarachnoid hemorrhage. Neurol Res25, 839–845, doi:10.1179/016164103771953934 (2003). [PubMed: 14669527]
18. Darwish H, Mahmood A, Schallert T, Chopp M & Therrien B Mild traumatic brain injury (MTBI) leads to spatial learning deficits. Brain Inj 26, 151–165, doi:10.3109/02699052.2011.635362 (2012). [PubMed: 22360521]
19. Yeo SS & Jang SH Neural reorganization following bilateral injury of the fornix crus in a patient with traumatic brain injury. J Rehabil Med 45, 595–598, doi:10.2340/16501977-1145 (2013). [PubMed: 23588891]
20. Tate DF & Bigler ED Fornix and hippocampal atrophy in traumatic brain injury. Learn Mem 7, 442–446, doi:10.1101/lm.33000 (2000). [PubMed: 11112803]

21. Ramlackhansingh AFet al.Inflammation after trauma: microglial activation and traumatic brain injury. Ann Neurol70, 374–383, doi:10.1002/ana.22455 (2011). [PubMed: 21710619]
22. Donat CK, Scott G, Gentleman SM & Sastre M Microglial Activation in Traumatic Brain Injury. Front Aging Neurosci 9, 208, doi:10.3389/fnagi.2017.00208 (2017). [PubMed: 28701948]
23. Azevedo EPet al.Activated microglia mediate synapse loss and short-term memory deficits in a mouse model of transthyretin-related oculoleptomeningeal amyloidosis. Cell Death Dis4, e789, doi:10.1038/cddis.2013.325 (2013). [PubMed: 24008733]
24. Elmore MRPet al.Replacement of microglia in the aged brain reverses cognitive, synaptic, and neuronal deficits in mice. Aging Cell17, e12832, doi:10.1111/acel.12832 (2018). [PubMed: 30276955]
25. Muccigrosso MMet al.Cognitive deficits develop 1month after diffuse brain injury and are exaggerated by microglia-associated reactivity to peripheral immune challenge. Brain Behav Immun54, 95–109, doi:10.1016/j.bbi.2016.01.009 (2016). [PubMed: 26774527]
26. Ritzel RMet al.Sustained neuronal and microglial alterations are associated with diverse neurobehavioral dysfunction long after experimental brain injury. Neurobiol Dis136, 104713, doi:10.1016/j.nbd.2019.104713 (2020). [PubMed: 31843705]
27. Bu Yet al.Mechanisms of hydrocephalus after intraventricular haemorrhage in adults. Stroke Vasc Neurol1, 23–27, doi:10.1136/svn-2015-000003 (2016). [PubMed: 28959460]
28. Ringstad G, Vatnehol SAS & Eide PK Glymphatic MRI in idiopathic normal pressure hydrocephalus. Brain 140, 2691–2705, doi:10.1093/brain/awx191 (2017). [PubMed: 28969373]
29. Ziegelitz Det al.Cerebral perfusion measured by dynamic susceptibility contrast MRI is reduced in patients with idiopathic normal pressure hydrocephalus. J Magn Reson Imaging39, 1533–1542, doi:10.1002/jmri.24292 (2014). [PubMed: 24006249]
30. Olopade FE, Shokunbi MT & Siren AL The relationship between ventricular dilatation, neuropathological and neurobehavioural changes in hydrocephalic rats. Fluids Barriers CNS 9, 19, doi:10.1186/2045-8118-9-19 (2012). [PubMed: 22938200]
31. Jackson PH & Lorber J Brain and ventricular volume in hydrocephalus. Z Kinderchir 39 Suppl 2, 91–93, doi:10.1055/s-2008-1044292 (1984).
32. Yu Z & Morrison B 3rd. Experimental mild traumatic brain injury induces functional alteration of the developing hippocampus. J Neurophysiol 103, 499–510, doi:10.1152/jn.00775.2009 (2010). [PubMed: 19923245]
33. Bain AC & Meaney DF Tissue-level thresholds for axonal damage in an experimental model of central nervous system white matter injury. J Biomech Eng 122, 615–622, doi:10.1115/1.1324667 (2000). [PubMed: 11192383]
34. Tang-Schomer MD, Patel AR, Baas PW & Smith DH Mechanical breaking of microtubules in axons during dynamic stretch injury underlies delayed elasticity, microtubule disassembly, and axon degeneration. FASEB J 24, 1401–1410, doi:10.1096/fj.09-142844 (2010). [PubMed: 20019243]
35. Garton TPet al.Hemoglobin-induced neuronal degeneration in the hippocampus after neonatal intraventricular hemorrhage. Brain Res1635, 86–94, doi:10.1016/j.brainres.2015.12.060 (2016). [PubMed: 26772987]
36. Strahle JMet al.Role of hemoglobin and iron in hydrocephalus after neonatal intraventricular hemorrhage. Neurosurgery75, 696–705; discussion 706, doi:10.1227/NEU.0000000000000524 (2014). [PubMed: 25121790]
37. Chen Zet al.Role of iron in brain injury after intraventricular hemorrhage. Stroke42, 465–470, doi:10.1161/STROKEAHA.110.602755 (2011). [PubMed: 21164132]
38. Yang Get al.A combination of serum iron, ferritin and transferrin predicts outcome in patients with intracerebral hemorrhage. Sci Rep6, 21970, doi:10.1038/srep21970 (2016). [PubMed: 26898550]
39. Dani C, Cecchi A & Bertini G Role of oxidative stress as physiopathologic factor in the preterm infant. Minerva Pediatr 56, 381–394 (2004). [PubMed: 15457136]

Highlights

- Pulsed rapid injections of blood into the lateral ventricle cause hydrocephalus, microglial reactivity and learning deficits.
- Steady-state pump infusions lead to hydrocephalus but not learning disorders.
- Dentate gyrus neurogenesis is not altered by intracranial blood or thrombin.

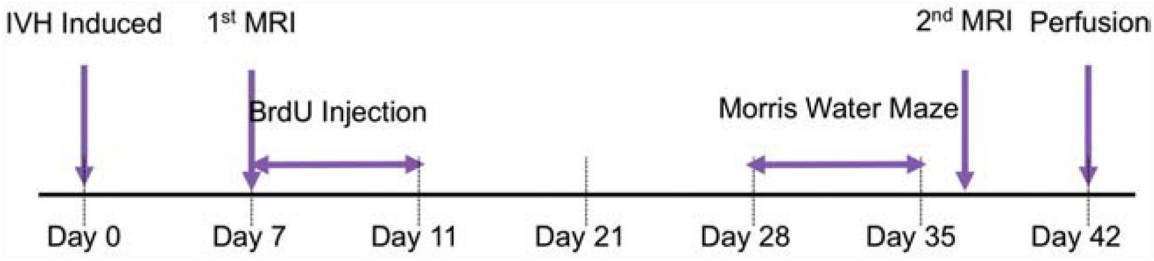

Figure 1.
Timeline of experimental workflow

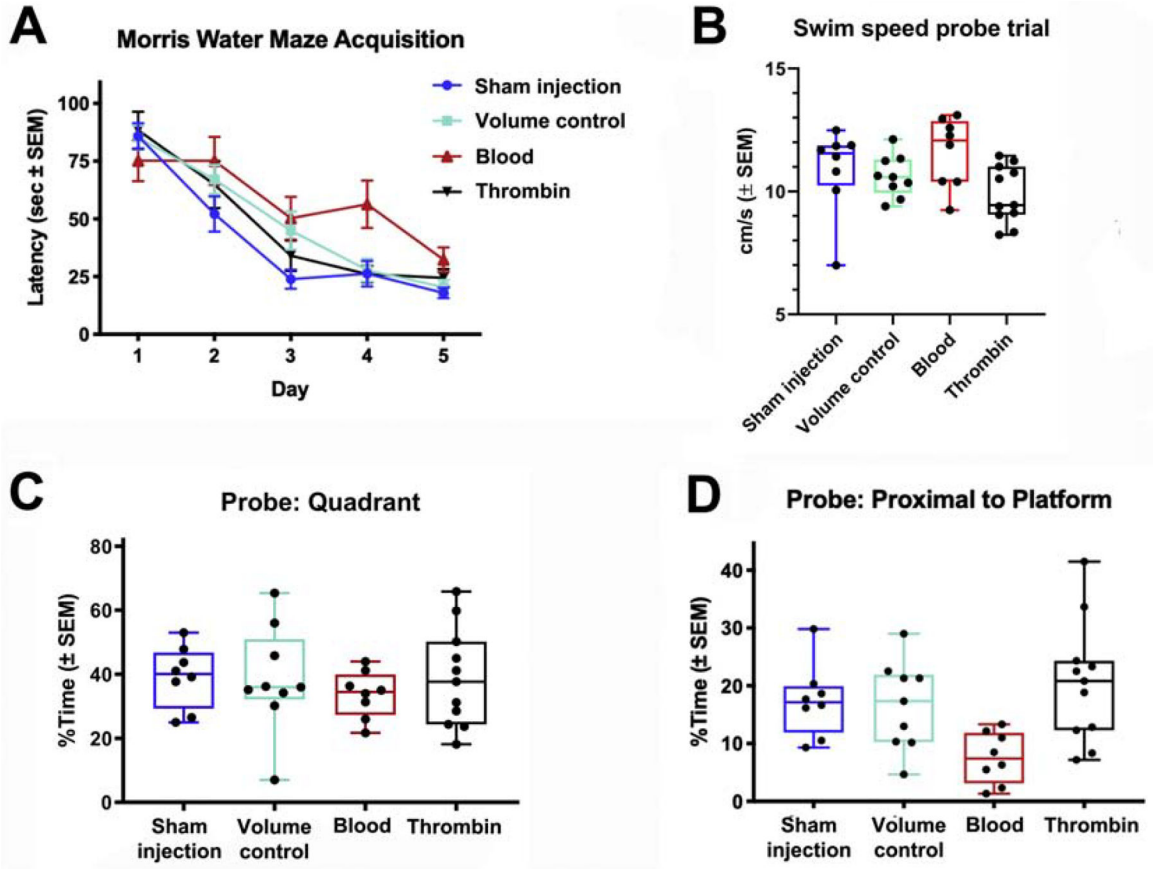

Figure 2.

Acquisition learning of rats 4 weeks after intervention in the Morris Water Maze (A). A 2-sided Dunnett post-hoc analysis identifies a significant increase in latency in rats with intraventricular blood compared to sham injections ($P<0.05$). Average swim speeds were unchanged between experimental groups (B). The quadrant probe trial does not show significant differences (C), but animals with intraventricular blood lack precision and spend significantly less time in the 10% area of the water maze around the platform on probe trial (D).

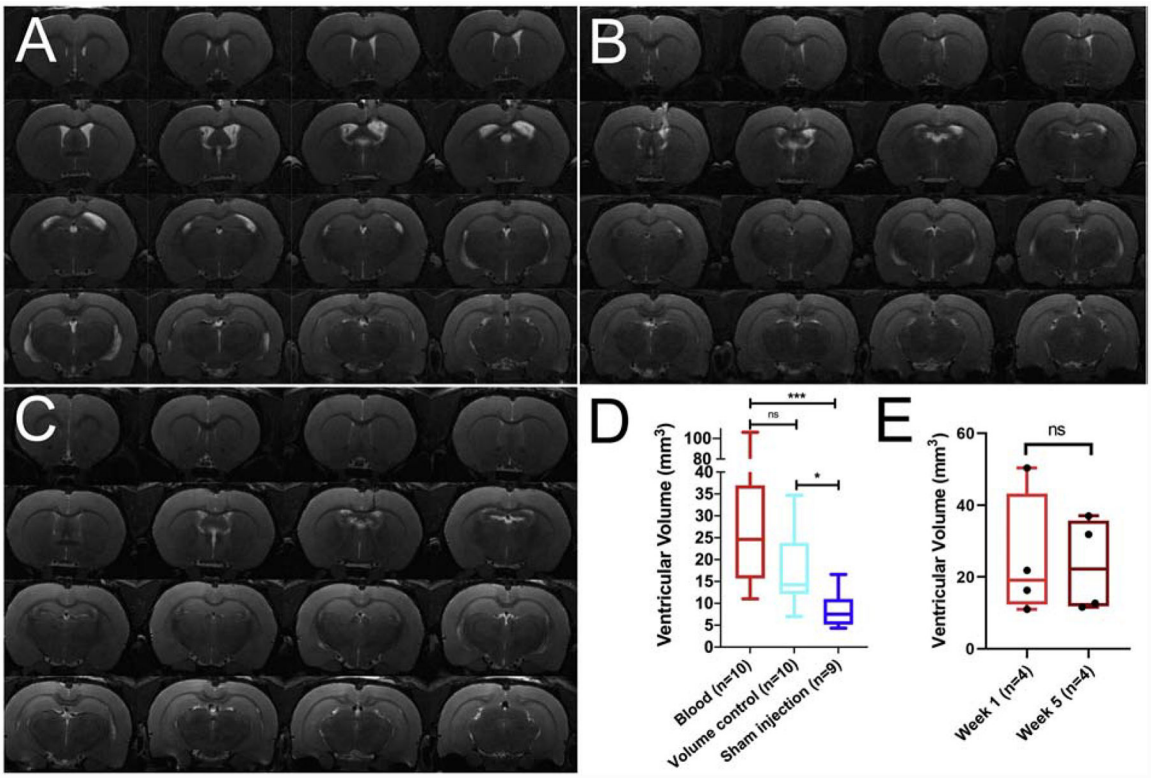

Figure 3.

T2-weighted MRI brain one week after pulsed hand-injections of 200 μl blood (A), 200 μl artificial CSF (volume control, B) or 5 μl artificial CSF (sham injection, C) into the right lateral ventricle over 2 minutes. Rapid injection of blood and volume lead to significantly larger ventricular sizes compared to sham injections (Dunn's multiple comparisons test, *** = $p < 0.001$, * = $p < 0.05$, ns = nonsignificant; D). Compared to week 1, the ventricles of animals with intraventricular blood do not significantly change in size around the time of water maze testing at week 5 (E). Whiskers: Minimal and maximal values; boxes: interquartile range; bar: median.

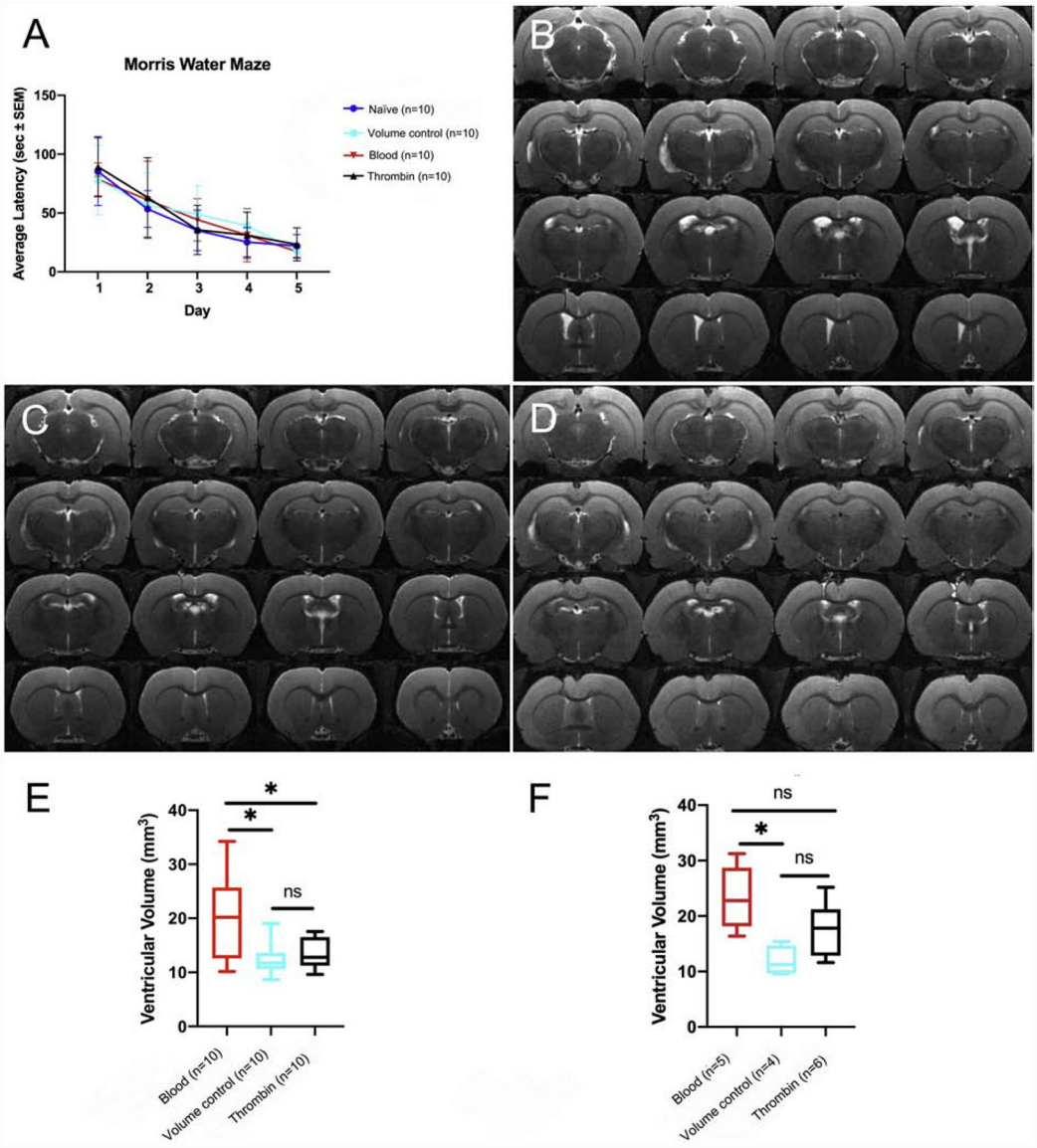

Figure 4.

Pump infusions of blood or thrombin into the lateral ventricle do not lead to worse memory acquisition than volume control or no surgery in the Morris Water Maze (A). Coronal MR images show that rats infused with blood into the lateral ventricle have hydrocephalus one week after infusion (B), but thrombin- and volume control-infused rats do not (C, D). Rats which were pump-infused with blood have significantly larger ventricles after 1 week (E) and 5 weeks (F) than aCSF infused animals (* = $p < 0.05$, ns = nonsignificant). Whiskers: Minimal and maximal values; boxes: interquartile range; bar: median.

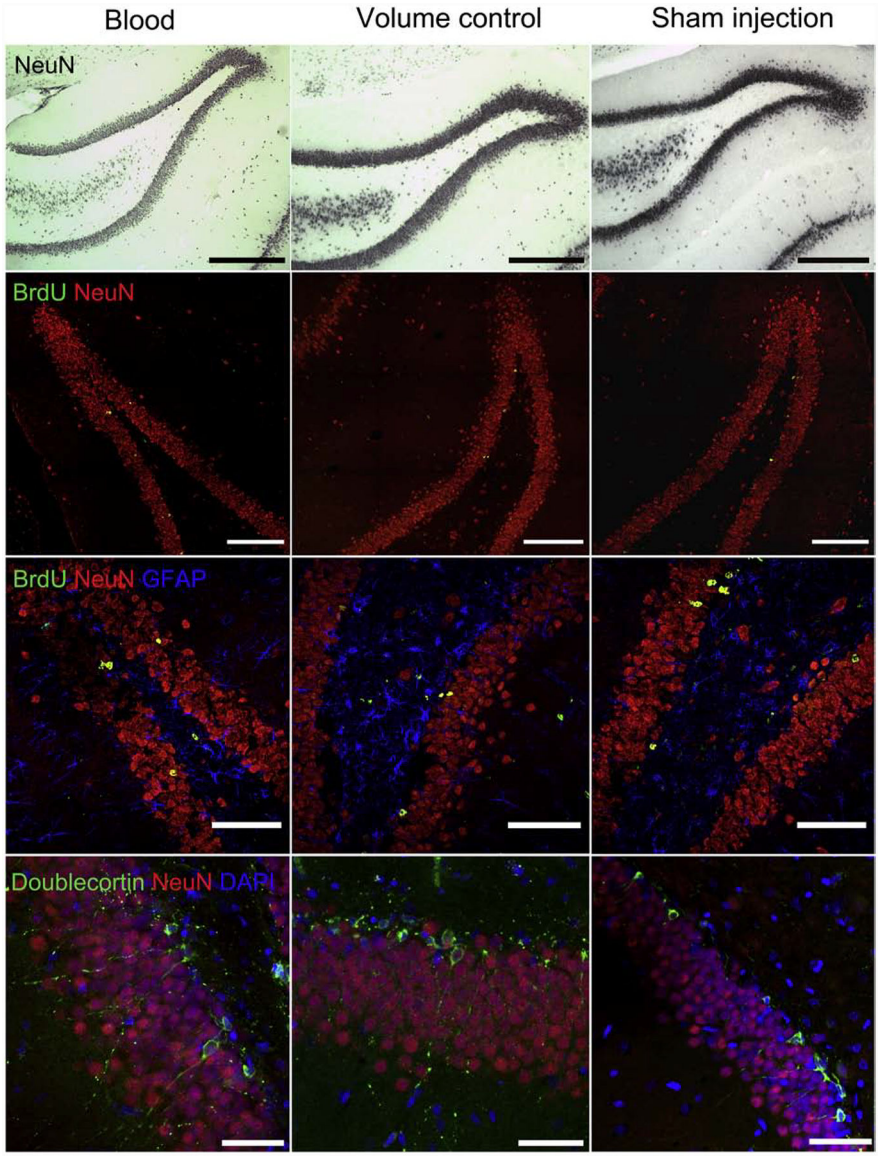

Figure 5.

Dentate gyrus neuronal survival is not changed between intraventricular blood, volume control and sham injection (first row, NeuN, black). There is also no difference in the number of BrdU-positive cells (second row, green) and differentiation into BrdU/NeuN-positive cells after 5 weeks (third row, BrdU, green, NeuN, red, GFAP, blue). There is no difference in the number of Doublecortin-positive cells after 5 weeks (fourth row: Doublecortin, green, NeuN, red, DAPI, blue). Scale bars: First row 500 μm; second row 200 μm; third row 100 μm; fourth row 50 μm

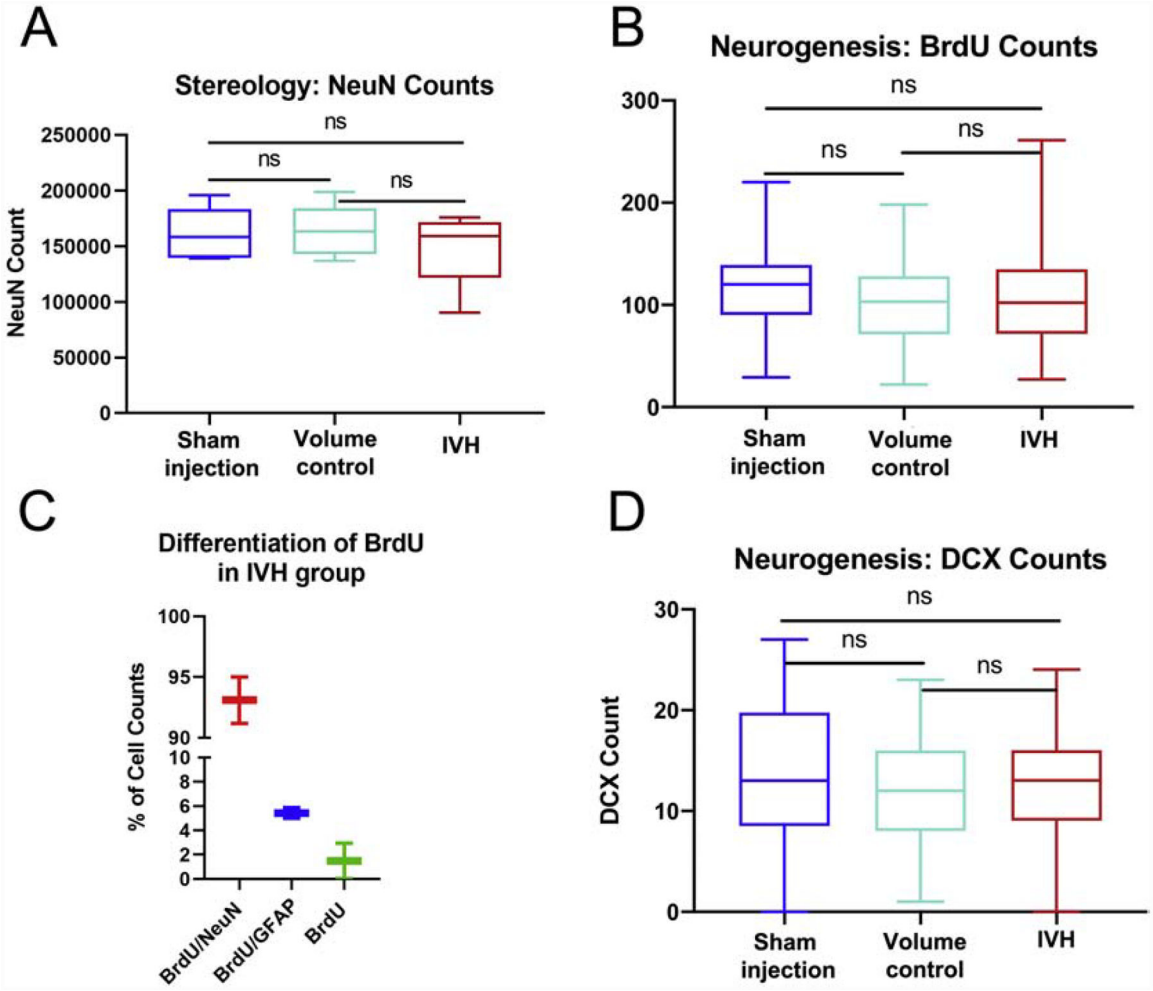

Figure 6.

There were no significant differences in neuronal counts in the granular zone of the dentate gyrus among the experimental groups so there was no evidence of neuronal death in the dentate gyrus after blood injection (A). The total number of BrdU-positive newly born cells was also unchanged between experimental groups (B). In the IVH group, there was no disturbance of neuronal differentiation since the vast majority (93%) of newly born progenitor cells differentiated into NeuN-positive neurons after 5 weeks (C). There was also no significant difference in the number of doublecortin-positive dentate progenitor cells across experimental groups after 5 weeks (D). Whiskers: Minimal and maximal values; boxes: interquartile range; bar: median.

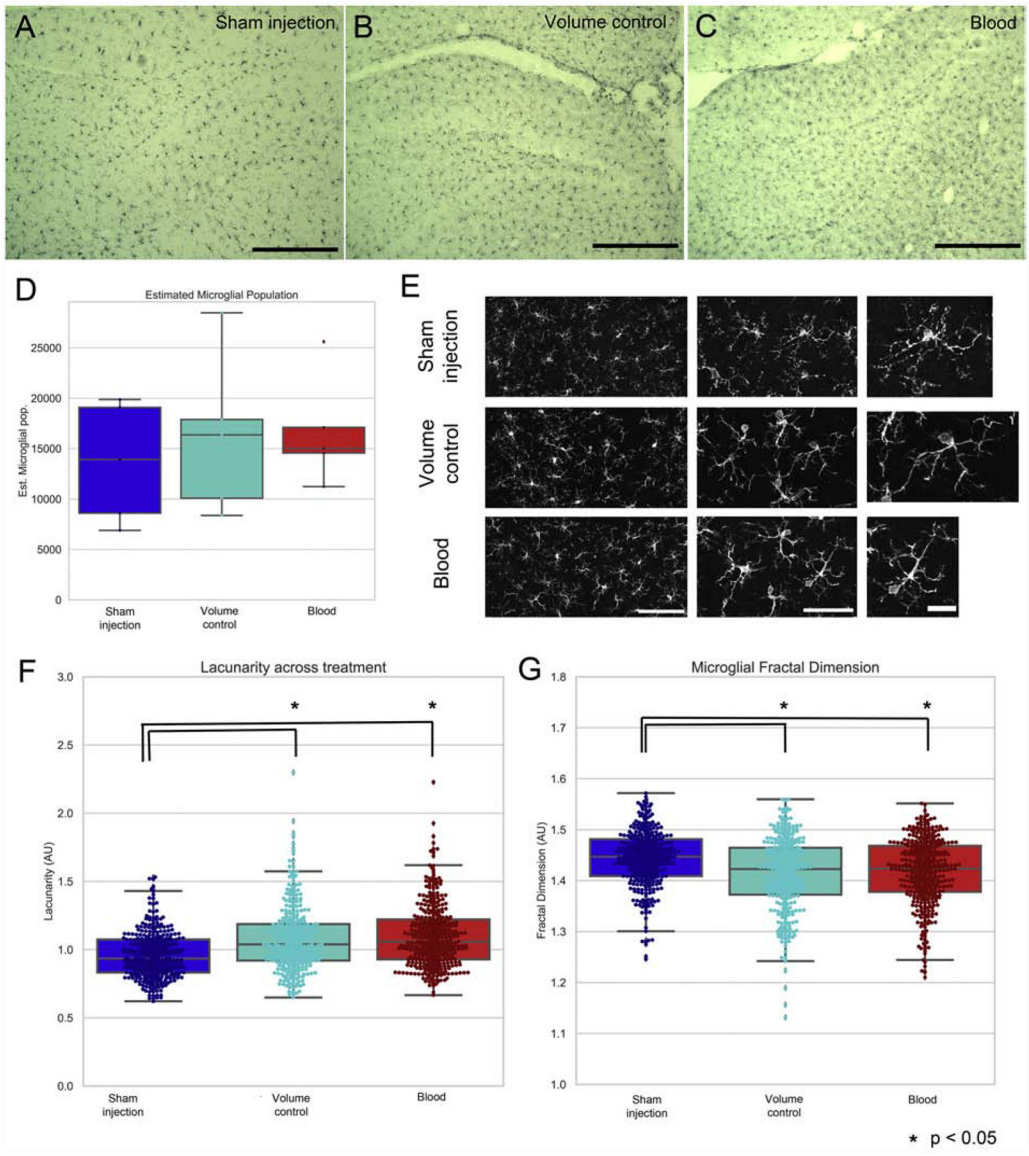

Figure 7.

Stereological analysis after staining for Iba-1 of sham (A), volume control (B) and blood pulsed injections (C) showed no significant differences in microglial proliferation in the dentate gyrus (D). Morphological analysis of the microglia (E) showed that blood and volume pulsed injections significantly increased microglial lacunarity (F) and significantly decreased microglial fractal dimension (G) indicating that pulsed injections of volume and blood led to microglial activation. Scale bars A-C: 500 μm; Scale bars E: First column 100 μm, second column 50 μm, third column 20 μm

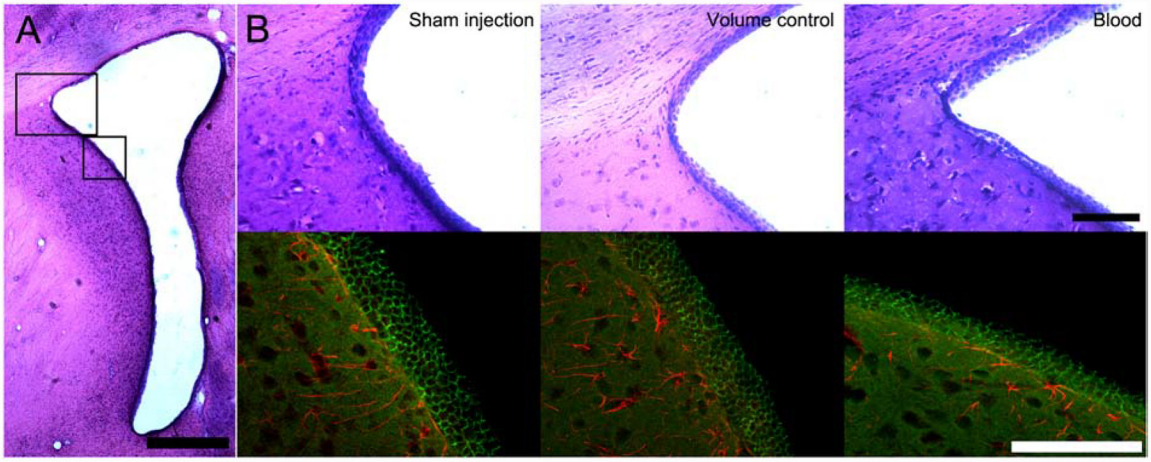

Figure 8.

A coronal H&E stained overview image of the lateral ventricle shows the location of representative sections taken from each group to analyse ependymal damage with H&E staining (large rectangle) and β-Catenin/GFAP (small rectangle below; A). No ependymal disruption or scar formation is found with H&E staining and β-Catenin/GFAP immunohistochemistry in any group, including rapid blood injections (B). Scale bar A: 500 μm. Scale bars B: 100 μm